

TOROIDAL EMBEDDINGS OF CUBIC PROJECTIVE PLANE OBSTRUCTIONS

MARIE KRAMER

ABSTRACT. Work of Glover and Huneke shows that a cubic graph embeds into the real projective plane if and only if it does not contain one of six topological minors called cubic projective plane obstructions. Here we classify up to equivalence the embeddings of these graphs into the torus.

INTRODUCTION

Kuratowski’s Theorem is a classical result: A graph is planar if and only if it does not contain K_5 or $K_{3,3}$ as a topological minor, that is, a subgraph isomorphic to a subdivision K_5 or $K_{3,3}$ [Kur30]. We say K_5 and $K_{3,3}$ are the topological obstructions for the plane.

Via stereographic projection, embeddability into the plane is equivalent to embeddability into the 2-sphere. Hence, $\{K_5, K_{3,3}\}$ is the complete set of topological obstructions for the orientable surface of genus zero. This raises the question of embedding these graphs into other surfaces. Gagarin, Kocay, and Neilson have shown that up to equivalence there are six embeddings of K_5 into the torus and two embeddings of $K_{3,3}$ [GKN03]. Similarly, Mohar proved that up to equivalence there are two embeddings of K_5 into the projective plane and one embedding of $K_{3,3}$ [Moh93].

In general, it is easy to see that obstructions for the orientable surface of genus n embed into the orientable surface of genus $n + 1$. Besides some elementary observations (see for example §4.4 in [MT01]), there seems to be less known about the relation between embeddability into orientable surfaces and nonorientable surfaces. One result in this area due to Fiedler, Huneke, Richter, and Robertson shows how to compute the orientable genus for graphs embeddable into the projective plane [FHRR95].

Work by Archdeacon, Glover, Huneke, and Wang gives an analogue to Kuratowski’s Theorem for the projective plane: There are 103 topological obstructions for the projective plane, six of which are cubic [GH75], [GHW79], [Arc81].

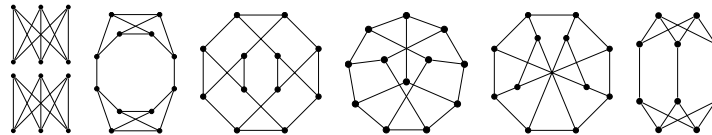


FIGURE 1. The six cubic projective plane obstructions

In this paper, we investigate the embeddability of the six cubic projective plane obstructions into the torus. We will refer to these by E_{42} , F_{11} , F_{12} , F_{13} , F_{14} , G_1 following the notation used in [GHW79] and [MT01].

Theorem A. *The graph E_{42} does not embed into the torus, the graph F_{12} embeds into the torus in exactly four ways up to equivalence, and each of the remaining four cubic projective plane obstructions embeds into the torus in exactly two ways up to equivalence.*

We refer to the Appendix for illustrations of the embeddings. Theorem A is proved in Lemma 1 for the case of E_{42} and in Sections 3 – 7 for the other five graphs.

Efforts have been made to obtain a complete list of obstructions for the torus, but no such list has been found yet. However, there are a number of partial results. There are currently over 250,000 known topological torus obstructions [MW18]. Chambers has investigated cubic torus obstructions with the aid of computers [Cha02], and it is believed that his list of 206 cubic obstructions is complete [MW18]. One application of Theorem A is to provide an independent proof that this list is indeed complete for small Betti numbers. This will be the subject of future work.

Further motivation for this work comes from an application to Riemannian geometry discovered by Kennard, Wiemeler and Wilking in [KWW]. More specifically, if a graph embeds into a surface, one obtains bounds on its systole. These systole bounds give bounds on matroid theoretic invariants, which in turn give geometric bounds for special tours representations. It turns out that cubic graphs represent extreme cases in the context of systole bounds and are therefore of high interest. While we restrict our attention to cubic graphs in this paper, we imagine a similar strategy would work to classify the embeddings into the torus of the remaining topological projective plane obstructions.

Acknowledgements. The author is grateful for support from NSF Research Grants DMS-2005280 and DMS-2402129, as well as from the Syracuse University Graduate School through Pre-Dissertation and Dissertation Fellowships in Summer 2023 and Summer 2024, respectively. The author would like to thank her advisor Dr. Lee Kennard for the invaluable advice, continued support, and stimulating conversations.

1. PRELIMINARIES

Unless otherwise specified $G = (V, E)$ denotes an undirected, simple graph. Most of the graphs we work with are **cubic**, that is, each of their vertices has degree three.

An **embedding** of a graph G into a surface Σ is a function φ mapping the vertices of G to points in Σ , and the edges of G to continuous curves in Σ , such that curves representing distinct edges intersect only at images of vertices (see §15.1 in [KK17]). We denote an embedding by $\varphi : G \hookrightarrow \Sigma$. A **face** of an embedding is a connected component of $\Sigma \setminus \varphi(G)$. A **facial cycle** or **facial walk** is an oriented cycle or walk in G along the boundary of a face of $\varphi(G)$.

A graph G is a **(topological) obstruction** for a surface Σ if G does not embed into Σ but every (topological) minor does. Here, a **topological minor** is a graph obtained from G by deleting edges and/or vertices and contracting edges with an endpoint of degree two. In other words, a graph is a topological minor of G if it has a subdivision isomorphic to a subgraph of G . A graph is a **cubic obstruction** for a surface Σ if it is cubic and a topological obstruction for Σ . We observe that if G and H are cubic graphs, H is a topological minor of G if and only if H is a minor of G . Hence, restricted to the class of cubic graphs, topological obstructions and obstructions are equivalent.

Two embeddings φ_1 and φ_2 of a graph G into a surface Σ are **equivalent** if there exists a homeomorphism $h : \Sigma \rightarrow \Sigma$ such that $\varphi_1(G) = (h \circ \varphi_2)(G)$ (see §15.2 in [KK17]). That is, there exists a homeomorphism mapping the image of G under φ_2 to the image of G under φ_1 . Since any homeomorphism of a surface maps facial walks to facial walks, two embeddings with facial walks of different lengths cannot be equivalent.

2. EMBEDDINGS OF $K_{3,3}$ INTO THE TORUS

It is well known that $K_{3,3}$ is the only cubic obstruction for the plane, as shown by Kuratowski [Kur30]. It is also known that the embedding of $K_{3,3}$ into the projective plane is unique up to equivalence [Moh93]. Similarly, $K_{3,3}$ embeds into the torus, and there are exactly two such embeddings up to equivalence [GKN03]. Observe that the embedding on the left in Figure 2 has two facial 4-cycles and one facial 10-cycle, while the embedding on the right has three facial 6-cycles.

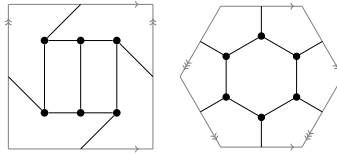


FIGURE 2. $K_{3,3}$ in the torus

Notice that each face of the toroidal embeddings of $K_{3,3}$ is homeomorphic to the plane, so the proof of Theorem A for the graph E_{42} follows immediately.

Lemma 1. *There are no embeddings of E_{42} into the torus.*

Proof. Recall that $E_{42} = K_{3,3} \sqcup K_{3,3}$. As seen in [GKN03], there are exactly two inequivalent embeddings of $K_{3,3}$ into the torus, pictured in Figure 2. Therefore, one copy of $K_{3,3}$ is embedded into the torus in one of those two ways and the second copy has to be embedded into one of the faces. In both cases, each face of the embedding is homeomorphic to a disk. As $K_{3,3}$ is nonplanar by [Kur30], it follows that E_{42} does not embed into the torus. \square

Remark. Alternatively, it follows from [BHK62] that E_{42} is one of the disconnected torus obstructions. Note that this implies that E_{42} embeds into the double torus, the orientable surface of genus two.

In order to prove Theorem A for the other five cubic projective plane obstructions, we use a classification of (directed) edged embeddings of $K_{3,3}$ into the torus. By an *edged embedding*, we mean an embedding of $K_{3,3}$ with one highlighted edge. In a *directed edged embedding*, the highlighted edge has an orientation. We will first prove a statement about the number of directed edged embeddings. The analogous statement about the number of edged embeddings will then follow immediately.

Lemma 2. *There are exactly six inequivalent directed edged embeddings of $K_{3,3}$ into the torus.*

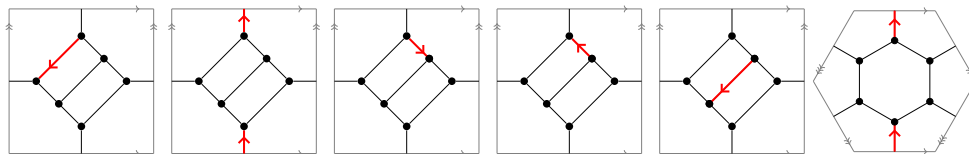


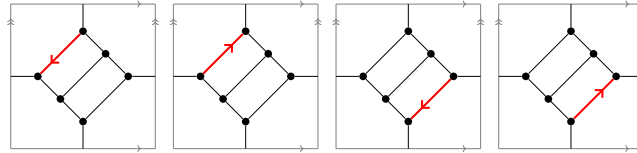
FIGURE 3. The six directed edged embeddings $(K_{3,3}, \vec{e}) \hookrightarrow T^2$

Proof. We will start by showing that there are at most six equivalence classes of directed edged embeddings of $K_{3,3}$ into the torus. Note that $K_{3,3}$ has nine edges, so there are

eighteen ways to select and orient an edge. However, we will see that many of these choices result in equivalent embeddings.

First, consider the embedding of $K_{3,3}$ into the torus pictured on the left in Figure 2. We will use the following two homeomorphisms of the torus to prove the below claims: A rotation ρ by 180° , and a reflection r along the diagonal from the bottom left to the top right. Note that these operations map the image of $K_{3,3}$ to the image of $K_{3,3}$. Embeddings related by these operations are thus equivalent according to the definition in Section 1.

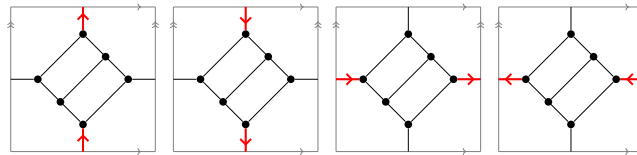
Claim 1. The four directed edged embeddings $(K_{3,3}, \vec{e}) \hookrightarrow T^2$ shown below are equivalent.



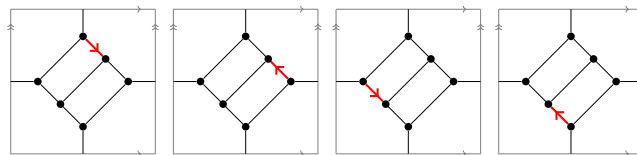
Proof. The first and fourth embedding, and the second and third one are related by a rotation by 180° , respectively. The first and third embedding, and the second and fourth one are related by the above mentioned reflection r , respectively. ■

Arguing similarly, we easily get Claims 2 – 5 below.

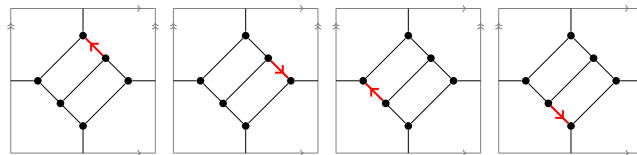
Claim 2. The four directed edged embeddings $(K_{3,3}, \vec{e}) \hookrightarrow T^2$ shown below are equivalent.



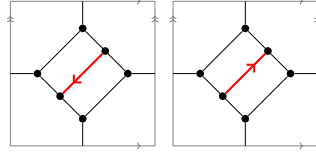
Claim 3. The four directed edged embeddings $(K_{3,3}, \vec{e}) \hookrightarrow T^2$ shown below are equivalent.



Claim 4. The four directed edged embeddings $(K_{3,3}, \vec{e}) \hookrightarrow T^2$ shown below are equivalent.

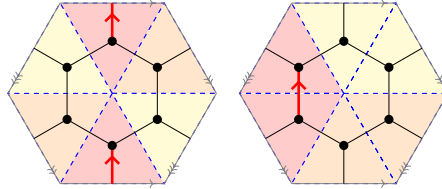


Claim 5. The two directed edged embeddings $(K_{3,3}, \vec{e}) \hookrightarrow T^2$ shown below are equivalent.



Remark. Note that the automorphism group of $K_{3,3}$ is $(S_3 \times S_3) \rtimes \mathbb{Z}_2$, where \mathbb{Z}_2 acts by interchanging the S_3 factors. The homeomorphisms ρ and r of the embedding of $K_{3,3}$ in the left of Figure 2 induce a subgroup of order four of the automorphism group of $K_{3,3}$. More specifically, the group generated by ρ and r is of the form $\langle \rho, r \mid \rho^2 = r^2 = e, \rho r \rho^{-1} = r \rangle \cong \mathbb{Z}_2 \times \mathbb{Z}_2$. Lastly, Claims 1 – 5 give that the action of $\mathbb{Z}_2 \times \mathbb{Z}_2$ on the 18-element set of oriented edged embeddings of $K_{3,3}$ into the torus has four orbits of size four, and one orbit of size two.

Next, we consider the embedding of $K_{3,3}$ into the torus pictured on the right in Figure 2. We will use the following two homeomorphisms of the torus to prove the claim below: A counterclockwise rotation by 60° , and the operation ε obtained by cutting the torus into six triangular regions and pasting them back together as pictured below. Note that both of these operations map the the image of $K_{3,3}$ to the image of $K_{3,3}$.



Claim 6. All 18 directed edged embedding $(K_{3,3}, \vec{e}) \hookrightarrow T^2$ with underlying embeddings as on the right of Figure 2 are equivalent.

Proof. The homeomorphism ε shows the equivalence of a directed edged embedding with \vec{e} being one of the six edges of the central hexagon to one with \vec{e} being one of the other three edges. Moreover, in composition with counterclockwise rotations by 60° , ε can be used to reverse the direction of a directed edge in the central hexagon. Finally, repeated application of counterclockwise rotations by 60° gives the remaining desired equivalences. ■

Remark. These homeomorphisms induce automorphisms of $K_{3,3}$. The subgroup of automorphisms that can be realised by this embedding of $K_{3,3}$ into the torus is isomorphic to $S_3 \times S_3$, however it is not the the standard such subgroup $(S_3 \times S_3) \times 1 \leq (S_3 \times S_3) \rtimes \mathbb{Z}_2$.

Combining Claims 1 – 6 gives that there are at most six inequivalent embeddings. It remains to show that the embeddings pictured in Figure 3 are pairwise inequivalent. Since Embedding 6 is the only one with facial 6-cycles and homeomorphisms of the torus map facial cycles to facial cycles, Embedding 6 cannot be equivalent to any of the other embeddings. Observe that in Embeddings 1 through 5 there are exactly two edges that appear in the facial 10-cycle twice. Such an edge has to get mapped to such an edge under homeomorphisms of the torus. In particular, Embedding 2 cannot be equivalent to any of the other four remaining ones. Similarly, in Embeddings 1 through 5 there exists a unique edge separating the two facial 4-cycles. Any homeomorphism of the torus has to map this edge to itself. This implies in particular that Embedding 5 cannot be equivalent to any of the other three remaining embeddings. It remains to compare Embeddings 1, 3, and 4. In Embedding

1, neither the starting point nor the endpoint \vec{e} are part of both facial 4-cycle. In Embedding 3, the endpoint of \vec{e} is part of both facial 4-cycles, and in Embedding 4 the starting point of \vec{e} is part of both facial 4-cycles. This implies that Embeddings 1, 3, and 4 are pairwise inequivalent, finishing the proof. \square

Lemma 3. *There are exactly five inequivalent edged embeddings of $K_{3,3}$ into the torus.*

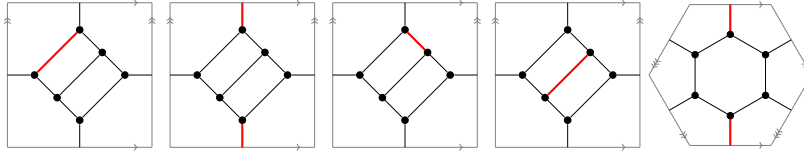


FIGURE 4. The five edged embeddings $(K_{3,3}, e^*) \hookrightarrow T^2$

Proof. This follows directly from Lemma 2 by disregarding the orientation. In particular, Embeddings 3 and 4 in Figure 3 are the same if we delete the orientation. \square

In addition to (directed) edged embeddings, we will use the notion of a *cycled embedding*. By this, we mean an embedding of $K_{3,3}$ into the torus with a highlighted 4-cycle.

Lemma 4. *There are exactly five inequivalent cycled embeddings of $K_{3,3}$ into the torus.*

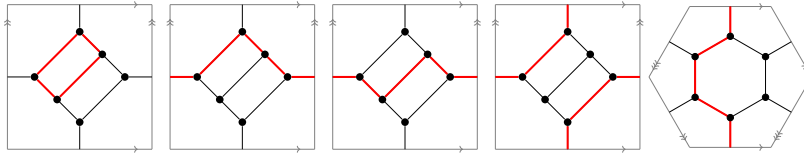
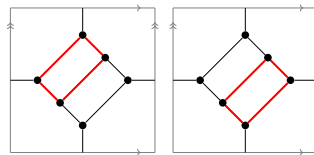


FIGURE 5. The five cycled embeddings $(K_{3,3}, C_4) \hookrightarrow T^2$

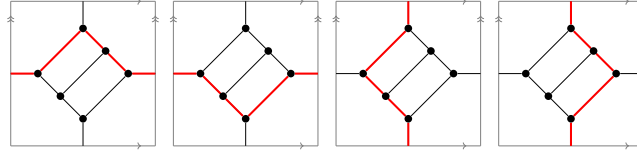
Proof. Similar to the proof of Lemma 2, we will start by showing that there are at most five equivalence classes of cycled embeddings of $K_{3,3}$ into the torus. Note that there are nine distinct 4-cycles in $K_{3,3}$: Let $V(K_{3,3}) = V_1 \cup V_2$ be the partition of vertices of $K_{3,3}$. Any 4-cycle contains exactly two vertices from V_1 and two vertices from V_2 . Thus, the total number of choices for the set of vertices of a 4-cycle is $\binom{3}{2} \cdot \binom{3}{2} = 9$. Once the vertices of $C_4 \subset K_{3,3}$ are fixed, the edges of C_4 are completely determined.

First, we consider the embedding of $K_{3,3}$ into the torus pictured on the left of Figure 2. Recall the homeomorphisms ρ , the rotation by 180° , and r , the reflection along the diagonal from the bottom left to the top right, used in the proof of Lemma 2. The next three claims follow as in the proof of Lemma 2, so we omit the proofs.

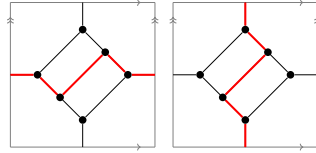
Claim 7. The two cycled embeddings $(K_{3,3}, C_4) \hookrightarrow T^2$ shown below are equivalent.



Claim 8. The four cycled embeddings $(K_{3,3}, C_4) \hookrightarrow T^2$ shown below are equivalent.



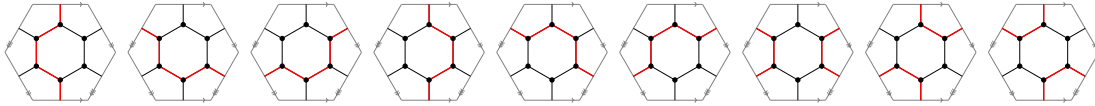
Claim 9. The two cycled embeddings $(K_{3,3}, C_4) \hookrightarrow T^2$ shown below are equivalent.



Remark. The action of $\mathbb{Z}_2 \times \mathbb{Z}_2$ on the 9-element set of cycled embeddings of $K_{3,3}$ into the torus has two orbits of size two, one orbit of size four, and one orbit of size one.

Next, we consider the embedding of $K_{3,3}$ into the torus pictured on the right in Figure 2. As in the proof of Lemma 2, we will use the counterclockwise rotation by 60° and the homeomorphism ε .

Claim 10. All nine cycled embeddings $(K_{3,3}, C_4) \hookrightarrow T^2$ shown below are equivalent.



Proof. Going from left to right, we can obtain the first six embeddings from the first one by a counterclockwise rotation by an integer multiple of 60° . We can obtain the seventh embedding from the first one by an application of ε . The final two embeddings can be obtained from the seventh one by a counterclockwise rotation by an integer multiple of 60° . Since equivalence of embeddings is an equivalence relation, the claim follows. ■

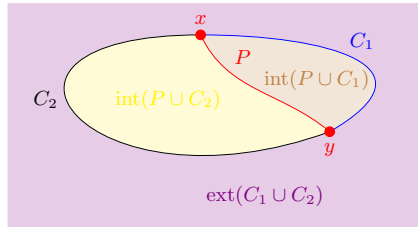
Combining Claims 7 – 10 implies that there are at most five inequivalent embeddings. It remains to show that the embeddings pictured in Figure 5 are pairwise inequivalent. Since Embedding 5 is the only one with facial 6-cycles, Embedding 5 cannot be equivalent to any of the other embeddings. Observe that in Embeddings 1 through 4 there are exactly two edges that appear in the facial 10-cycle twice. Such an edge has to get mapped to such an edge under homeomorphisms of the torus. In particular, as Embedding 4 is the only one whose highlighted 4-cycle uses both of these edges, it cannot be equivalent to any of the other three remaining ones. Similarly, in Embeddings 1 through 4 there exists a unique edge separating the two facial 4-cycles. Any homeomorphism of the torus has to map this edge to itself. This implies in particular that Embedding 2 cannot be equivalent to any of the other two remaining ones as the highlighted 4-cycle in embedding 2 does not use that edge. It remains to compare Embeddings 1 and 3. In Embedding 3, the highlighted 4-cycle uses an edge appearing twice in the facial 10-cycle, whereas the 4-cycle in Embedding 1 does not. This implies that Embeddings 1 and 3 are inequivalent, finishing the proof. □

3. TOROIDAL EMBEDDINGS OF F_{11}

In the remaining sections, we use repeatedly the following consequence of the Jordan Curve Theorem. A proof of the below proposition can be found in §2.2 in [MT01]. We present a different proof here.

Proposition 1. *Let C be a simple closed curve in \mathbb{R}^2 , $x, y \in C$, and $P : I \rightarrow \mathbb{R}^2$ a continuous path from x to y . Then $\mathbb{R}^2 \setminus (C \cup P)$ has three components.*

Proof. By the Jordan Curve Theorem, $C = C_1 \cup C_2$ separates the plane into two components, called the interior and exterior. In particular, the interior is nonempty. If P is on the interior of C , $P \cup C_1$ and $P \cup C_2$ are simple closed curves, and thus have a nonempty interior as well. Hence, we have the claimed three components.



The case of P being in the exterior of C may be reduced to the just covered case by stereographic projection. \square

Lemma 5. *There are exactly two inequivalent unlabelled embeddings of F_{11} into the torus.*

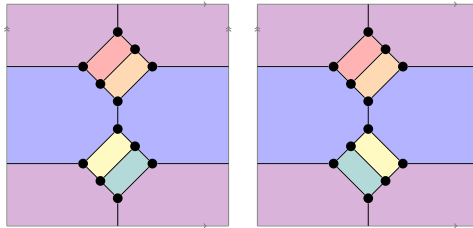
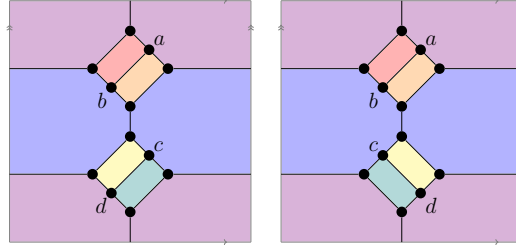
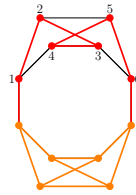


FIGURE 6. The two embeddings of F_{11} into the torus

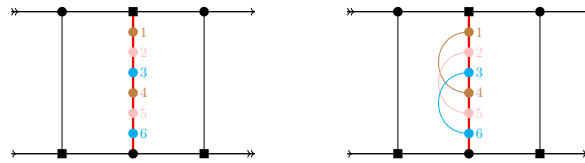
Remark. Both embeddings have four facial cycles of length four, and two facial cycles of length ten. To distinguish between the two, we observe that both embeddings have four vertices that are each part of two facial 4-cycles. We label these vertices a, b, c, d as shown in the figure below. Moreover, vertices a and d lie on a common facial cycle, and b and c lie on common facial cycle. Denote these by $C_L^{ad}, C_R^{ad}, C_L^{bc}$ and C_R^{bc} , respectively. We observe that on the one hand, vertices a and d have distance five in C_L^{ad} , and so do vertices b and c in C_L^{bc} . On the other hand, vertices a and d have distance three in C_R^{ad} , and so do vertices b and c in C_R^{bc} . Thus, the two embeddings cannot be equivalent. We will refer to the first of these two embeddings as the *5-embedding*, and the other as the *3-embedding*.



Proof. Since F_{11} is a cubic nonprojective graph, it is nonplanar and contains a subgraph homeomorphic to $K_{3,3}$. Furthermore, any subgraph homeomorphic to $K_{3,3}$ is embedded into the torus in one of the ways pictured in Figure 2. To classify the embeddings of F_{11} , we fix a subgraph H homeomorphic to $K_{3,3}$ as shown below. Note that $V(H) = V(F_{11})$ and $E(H) = E(F_{11}) \setminus \{(i, i + 3)\}_{i \in \{1,2,3\}}$. Let e^* denote the path of length seven in H containing the vertices 1 through 6.



The graph H is shown below, where $K_{3,3}$ is drawn as the Möbius ladder on three rungs. Once we have the pictured subdivision of $K_{3,3}$, there is a unique way to add the remaining edges to obtain F_{11} by recalling that F_{11} is cubic and has girth four.



By Lemma 3, there are five inequivalent edged embeddings $(K_{3,3}, e^*) \hookrightarrow T^2$. As described above, picking one edge in $K_{3,3}$ to be the edge e^* completely determines how to build F_{11} . Hence, we analyse the five cases below and check which ones can be extended to an embedding of F_{11} .

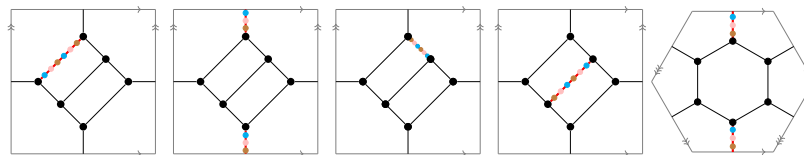
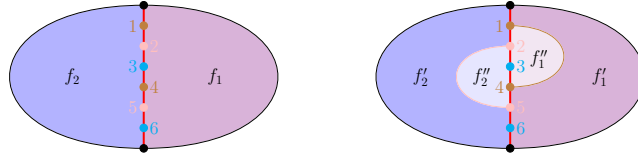


FIGURE 7. Subdivisions of $K_{3,3}$ in F_{11}

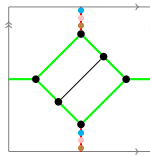
In Cases 1, 3, 4, and 5 of Figure 7 e^* is part of two distinct facial cycles bounding faces that are homeomorphic to a disk.

We may assume without loss of generality that the edge 14 goes through face f_1 . By Lemma 1 this cuts f_1 into two components f'_1 and f''_1 as pictured below. This forces the edge 25 to

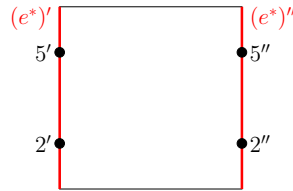
go through face f_2 , cutting it into two components f'_2 and f''_2 as pictured below. It is now impossible to add the final edge 36 as the vertex 3 is part of the facial cycles of f'_1 and f''_2 , whereas the vertex 6 is part of the facial cycles of f'_1 and f'_2 . Hence, these embeddings of a subdivision of $K_{3,3}$ cannot be extended to an embedding of F_{11} .



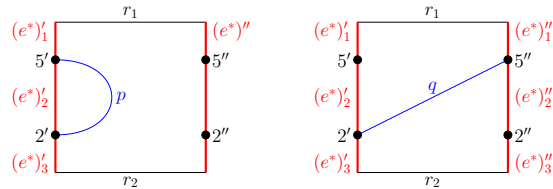
Case 2 in Figure 7 differs from the others as e^* is part of only one facial cycle. Note that cutting the torus along the highlighted edges of $K_{3,3}$ gives a cylinder.



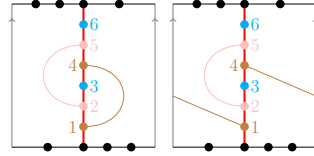
We now want to connect vertices 2 and 5 by an edge. Note that we may view a cylinder as a disk with part of the boundary identified along e^* . In particular, there are two copies of 2, namely $2'$ and $2''$ on the boundary of the disk, and two copies of 5, namely $5'$ and $5''$. Note that by symmetries of the cylinder, a path from $2'$ to $5'$ is equivalent to a path from $2''$ to $5''$. Similarly, a path from $2'$ to $5''$ is equivalent to one from $2''$ to $5'$.



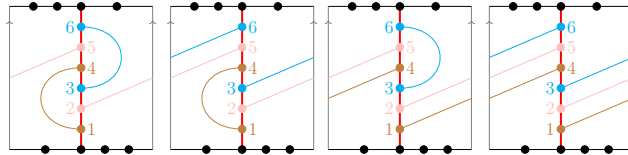
By Lemma 1, a simple continuous path p from $2'$ to $5'$ separates the interior of the disk into two components. One component has boundary $(e^*)'_2 \cup p$, while the other has boundary $(e^*)'_1 \cup r_1 \cup (e^*)'' \cup r_2 \cup (e^*)'_3 \cup p$. Similarly, a simple continuous path q from $2'$ to $5''$ separates the interior of the disk into two components. One component has boundary $(e^*)'_2 \cup (e^*)'_1 \cup r_1 \cup (e^*)'' \cup r_2 \cup (e^*)'_3 \cup q$, while the other has boundary $(e^*)''_2 \cup (e^*)''_3 \cup r_2 \cup (e^*)'_3 \cup q$. These components then correspond to components of the cylinder built from the usual quotient map.



As just established, adding the edge 25 cuts the cylinder into two components in one of two ways. We quickly see that in one of the cases, we cannot add the edge 36 after having added the edge 14 in either of the two possible ways, as shown below.



In the other case we similarly have two ways of drawing the edge 14. Moreover, once the edge 14 is drawn, there are two ways of drawing the edge 36. The four possible drawings are shown below.



Correspondingly, we have shown that all embeddings of F_{11} are equivalent to one of the four pictured below.

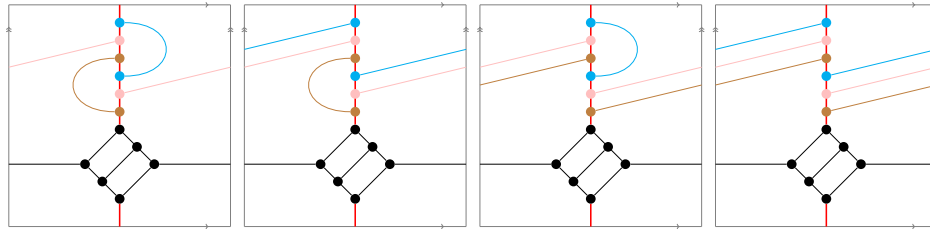


FIGURE 8. Extensions of $K_{3,3}$ embeddings to F_{11} embeddings

We will now show that each of the four embeddings of F_{11} into the torus in Figure 8 is equivalent to one of the two embeddings in Figure 6. To this end, we will decompose each of the two embeddings in Figure 6 into their facial n -gons and describe how to glue them together to obtain a torus. Then, we will show that each of the four embeddings in 8 can be decomposed and glued together in one of those two ways.

Consider the four squares and two decagons below. Note that each vertex appears three times, and each edge appears twice. Identifying vertices with the same label and edges between the same pair of vertices, we obtain the 5-embedding of F_{11} from Figure 6.

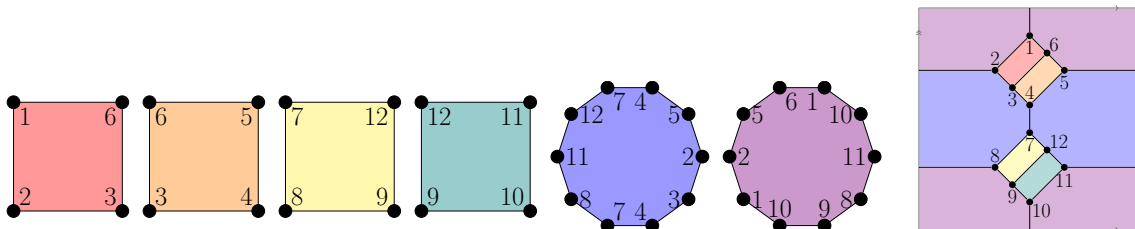
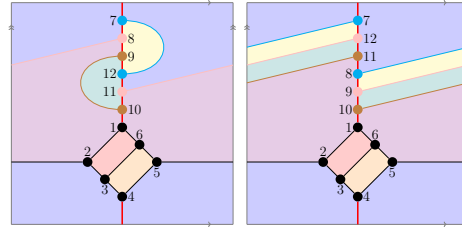


FIGURE 9. Decomposing the 5-embedding of F_{11}

We observe that we can decompose the embeddings of F_{11} in Figure 8 into four squares and two decagons. Moreover, we can label the vertices of the first and fourth embedding

and decompose the torus as in Figure 9. This implies the existence of a homeomorphism of the torus that realizes an equivalence of the embedding from this case and the known 5-embedding of F_{11} .



Next, consider the four squares and two decagons below. Note that each vertex appears three times, and each edge appears twice. Identifying vertices with the same label and edges between the same pair of vertices, we obtain the 3-embedding of F_{11} from Figure 6.

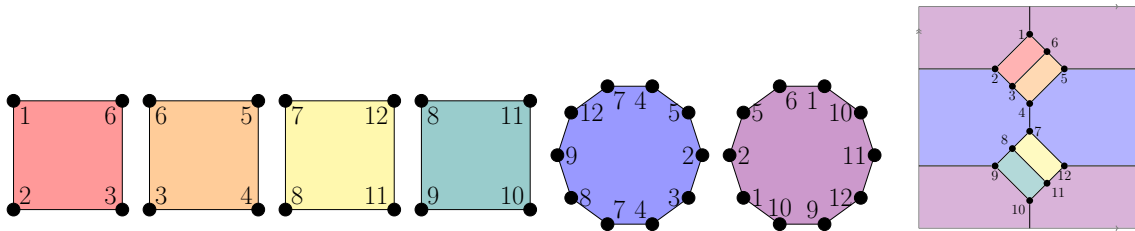
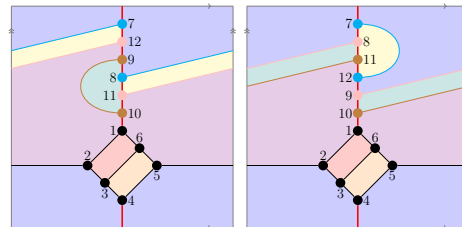


FIGURE 10. Decomposing the 3-embedding of F_{11}

Similarly to above, we can label the vertices of the second and third embedding in Figure 8 and decompose the torus as in Figure 10. This implies the existence of a homeomorphism of the torus that realizes an equivalence of the embedding from this case and the known 3-embedding of F_{11} .



We can now conclude that there are at most two inequivalent embeddings of F_{11} into the torus, namely the ones depicted in Figure 6. The remark preceding the proof of Lemma 5 implies that these two embeddings are inequivalent, finishing the proof.

□

4. TOROIDAL EMBEDDINGS OF F_{12}

Lemma 6. *There are exactly four inequivalent unlabelled embeddings of F_{12} into the torus.*

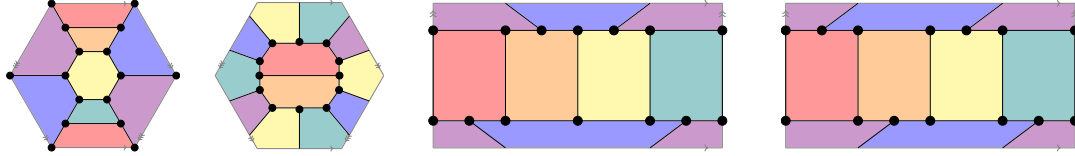
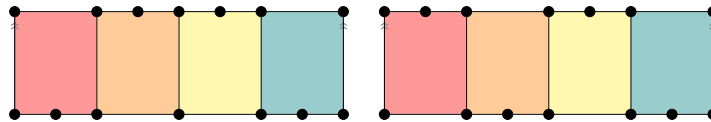


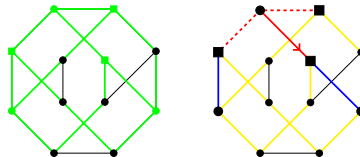
FIGURE 11. The four embeddings of F_{12} into the torus

Remark.

- (1) The first embedding from the left has two facial cycles of length four, two facial cycles of length six, and two facial cycles of length eight. In particular, it is the only embedding with a facial 6-cycle and thus cannot be equivalent to any of the other embeddings. We will refer to it as the *6-cycle embedding*.
- (2) The second embedding from the left has two facial cycles of length four, and four facial cycles of length seven. In particular, it is the only embedding with a facial 7-cycle and thus cannot be equivalent to any of the other embeddings. We will refer to it as the *7-cycle embedding*.
- (3) The remaining two embeddings both have four facial cycles of length five, and two facial cycles of length eight. To distinguish between the two, we observe that both embeddings contain a cylinder of 5-cycles, and each boundary component of that cylinder has two vertices of degree two. In one of the embeddings, the vertices of degree two in one boundary component belong to adjacent 5-cycles, whereas in the other they do not. More precisely, the distance between degree two vertices in a boundary component is two in one of the embeddings, and three in the other one. Thus, the two embeddings cannot be equivalent. We will refer to the first of these two embeddings as the *2-embedding* and the other one as the *3-embedding*.



Proof. We proceed similarly as in the proof of Lemma 5. Since F_{12} is a cubic nonprojective graph, it is nonplanar and contains a subgraph homeomorphic to $K_{3,3}$. Furthermore, any subgraph homeomorphic to $K_{3,3}$ is embedded into the torus in one of the ways pictured in Figure 2. To classify the embeddings of F_{12} , we fix a subgraph H homeomorphic to $K_{3,3}$ as shown below.



To build this subdivision of $K_{3,3}$, note that the directed red edge \vec{e} starts at the unique vertex of $K_{3,3}$ none of whose incident edges get subdivided. The remaining edges incident to the endpoint of \vec{e} get subdivided once. In the unique 4-cycle of this subdivision, choose a pair of disjoint edges and subdivide each of these twice. In Figure 12, we have coloured the other two edges of this 4-cycle in blue. Once we have the pictured subdivision of $K_{3,3}$, there is a unique way to add the remaining edges to obtain F_{12} . In particular, b has to be part of a

4-cycle that includes a blue edge. Thus, $bb' \in E(F_{12})$. Similarly, c has to part of a 4-cycle that includes a blue edge, implying that $cc' \in E(F_{12})$. This forces aa' to be the final edge.

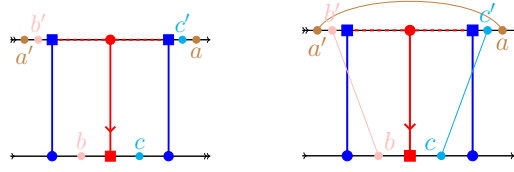


FIGURE 12. Building F_{12} from $K_{3,3}$

By Lemma 2, there are six inequivalent directed edged embeddings $(K_{3,3}, \vec{e}) \hookrightarrow T^2$. Note that picking the directed edge forces the location of the dashed red edges in Figure 12. Then there are two ways to choose the blue edges (once the first one is picked, the second is forced since they have to be disjoint). Thus, decorating the directed edged embeddings with the two blue edges e_1, e_2 , we get twelve *blue directed edged embeddings*, $(K_{3,3}, \vec{e}, \{e_1, e_2\}) \hookrightarrow T^2$. As described above, this completely determines F_{12} . Hence, we analyse the twelve cases below and check into which the remaining three edges aa', bb', cc' can be added.

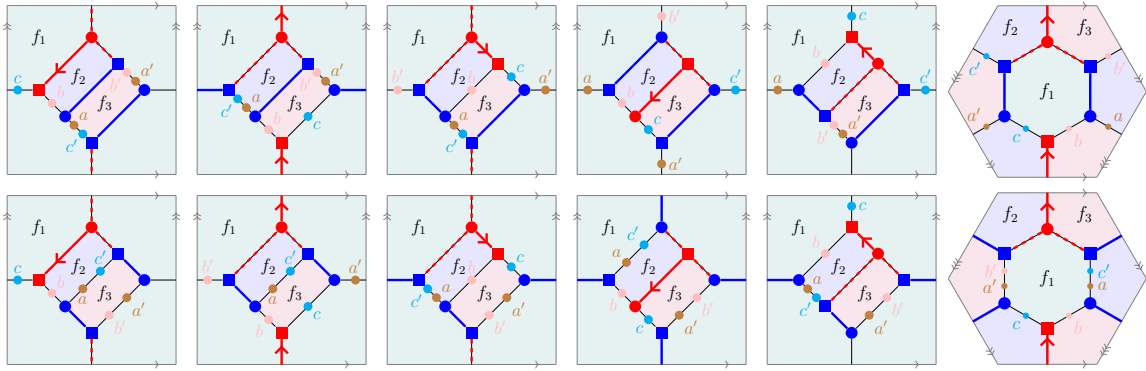


FIGURE 13. Subdivisions of $K_{3,3}$ in F_{12}

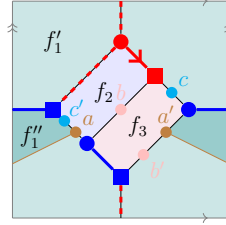
The cases are labelled 1a, 2a, etc. across the top row, and 1b, 2b, etc. across the bottom row. We immediately see the following:

- Case 1b: The edge cc' cannot be added. Thus, this embedding does not extend to an embedding of F_{12} .
- Case 2b: The edge aa' cannot be added. Thus, this embedding does not extend to an embedding of F_{12} .
- Case 3a: The edge bb' cannot be added. Thus, this embedding does not extend to an embedding of F_{12} .

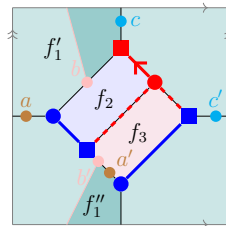
Note that since all embeddings of $K_{3,3}$ into the torus are cellular, each face is homeomorphic to a disk. Thus, if two vertices are on the boundary of a common face and neither of them appears more than once, there is a unique way to add an edge between the vertices up to equivalence.

We now consider the cases that will not result in embeddings of F_{12} :

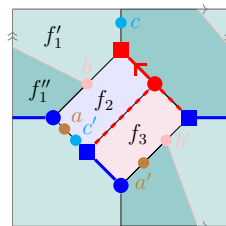
- Case 3b: f_1 is the unique face such that the vertices a and a' appear on its boundary, and each appears exactly once. Thus, there is a unique way up to equivalence to draw the edge aa' . However, now there is no face such that vertices c and c' appear on its boundary. Hence, we cannot extend the given embedding of a subdivision of $K_{3,3}$ to an embedding of F_{12} .



- Case 5a: f_1 is the unique face such that the vertices b and b' appear on its boundary, and each appears exactly once. Thus, there is a unique way to draw the edge bb' . However, now there is no face such that vertices a and a' appear on its boundary. Hence, we cannot extend the given embedding of a subdivision of $K_{3,3}$ to an embedding of F_{12} .

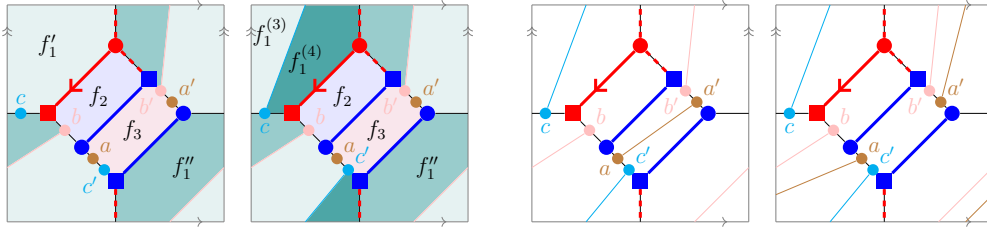


- Case 5b: Similar to the previous two cases, f_1 is the unique face such that vertices b and b' appear on its boundary, and each appears exactly once. However, now there is no face such that vertices a and a' appear on its boundary. Hence, we cannot extend the given embedding of a subdivision of $K_{3,3}$ to an embedding of F_{12} .

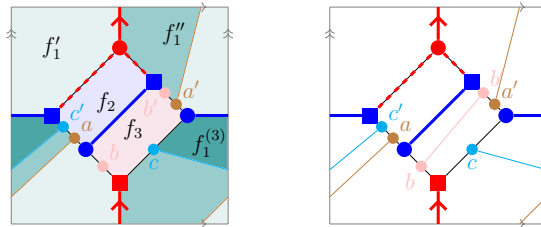


Finally, we proceed to the remaining cases, each of which gives at least one embedding of F_{12} into the torus.

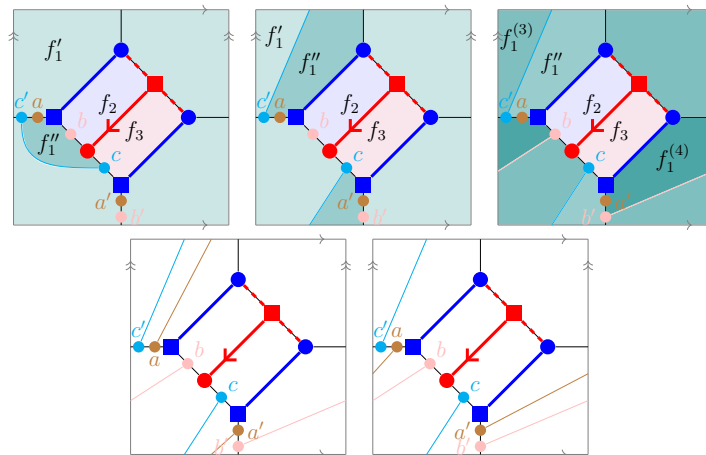
- Case 1a: f_1 is the unique face such that the vertices b and b' appear on its boundary, and each appears exactly once. Thus, there is a unique way to draw the edge bb' . This then forces the edge cc' to go through face f_1' . Finally, for the edge aa' there are two choices, giving the two embeddings of F_{12} pictured below.



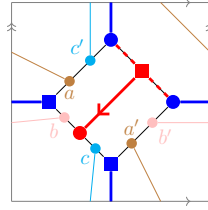
- Case 2a: f_1 is the unique face such that the vertices a and a' appear on its boundary, and each appears exactly once. Moreover, it is the only face with vertices c and c' on its boundary, and each appears exactly once. Thus, there is at most one way to draw the edges aa' , cc' . It is easy to check that it is indeed possible to draw both edges, as shown below. This then forces the edge bb' to go through face f_3 , and we get the embedding of F_{12} pictured below.



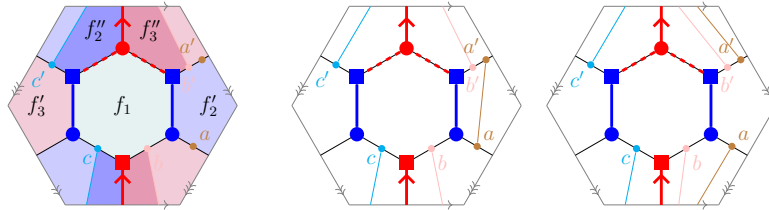
- Case 4a: f_1 is the unique face such that the vertices c and c' appear on its boundary, and vertex c' appears twice. Thus, there are two ways to draw the edge cc' . It is quick to see that one of these two options makes drawing the edge bb' impossible (left picture). Thus, we choose the other option (middle picture). Then there exists a unique way to draw the edge bb' as f_1' is the unique face such that both vertices appear on its boundary, and each appears exactly once. Finally, for the edge aa' there are two choices. Hence, we get the two embeddings of F_{12} pictured below.



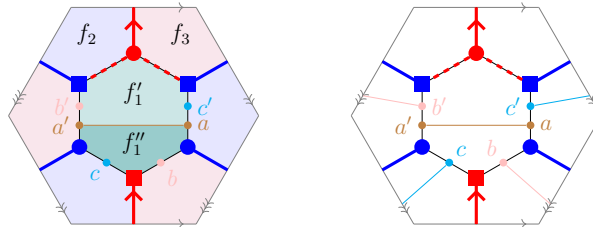
- Case 4b: Each of the vertices $a, a', b, b', c,$ and c' appears only on the boundary of face f_1 , and each appears exactly once. Thus, there is at most one way to draw all three edges aa' , bb' , cc' , pictured below.



- Case 6a: f_3 is the unique face such that the vertices b and b' appear on its boundary, and f_2 is the unique face such that the vertices c and c' appear on its boundary. Moreover, each appears exactly once. Thus, there is a unique way to draw the edges bb' and cc' . Finally, for the edge aa' there are two choices, giving the two embeddings of F_{12} pictured below.



- Case 6b: f_1 is the unique face such that the vertices a and a' appear on its boundary, and each appears exactly once. Thus, there is a unique way to draw the edge aa' . Now, f_3 is the unique face with vertices b and b' on its boundary, and f_2 is the unique face with vertices c and c' on its boundary. Moreover, each vertex appears exactly once on those boundaries. Thus, we get the embedding of F_{12} shown below.



Using the same technique as in Section 3, we will now show that each of these nine embeddings of F_{12} into the torus is equivalent to one of the four embeddings in Figure 11.

Consider the two squares, two hexagons, and two octagons below. Note that each vertex appears three times, and each edge appears twice. Identifying vertices with the same label and edges between the same pair of vertices, we obtain the 6-cycle embedding of F_{12} from Figure 11.

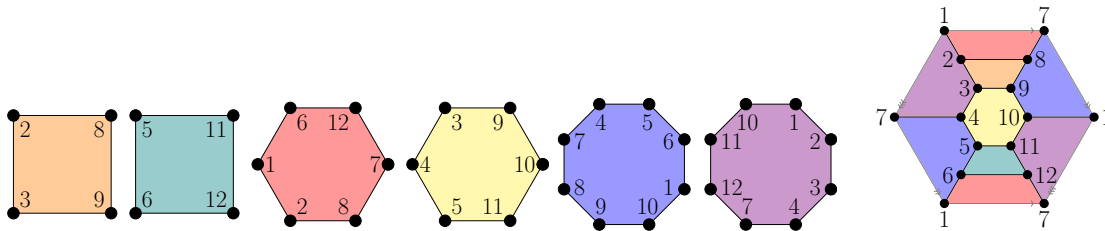
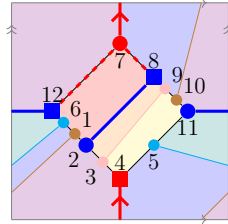


FIGURE 14. Decomposing the 6-cycle embedding of F_{12}

We now observe that we can decompose the embedding of F_{12} resulting from Case 2a into two squares, two hexagons, and two octagons. Moreover, we can label the vertices of this embedding and decompose the torus as in Figure 14. This implies the existence of a homeomorphism of the torus that realizes an equivalence of the embedding from this case and the known 6-cycle embedding of F_{12} .



Next, consider the two squares and four heptagons below. Identifying vertices with the same label and edges between the same pair of vertices, we obtain the 7-cycle embedding of F_{12} from Figure 11.

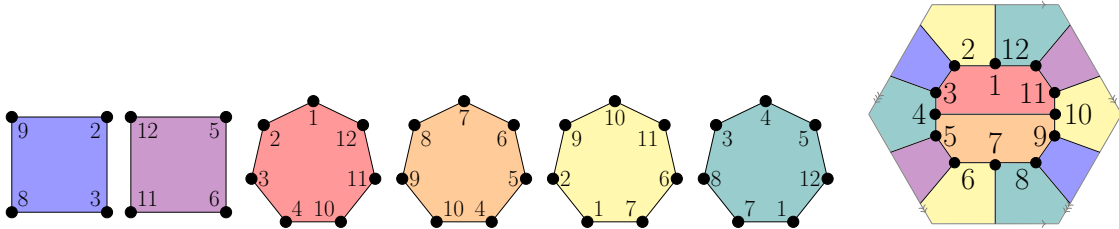
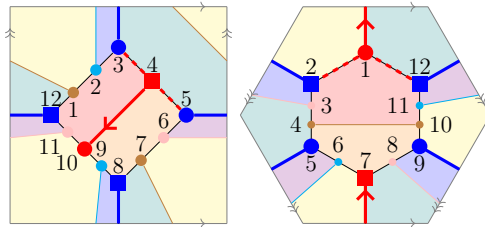


FIGURE 15. Decomposing the 7-cycle embedding of F_{12}

We observe that we can decompose the two embeddings of F_{12} resulting from Cases 4b and 6b into two squares, and four heptagons. Moreover, we can label the vertices of this embedding and decompose the torus as in Figure 15. Hence, the embeddings from these cases are equivalent to the known 7-cycle embedding of F_{12} .



Consider the four pentagons and two octagons. Identifying vertices with the same label and edges between the same pair of vertices, we obtain the 2-embedding of F_{12} from Figure 11.

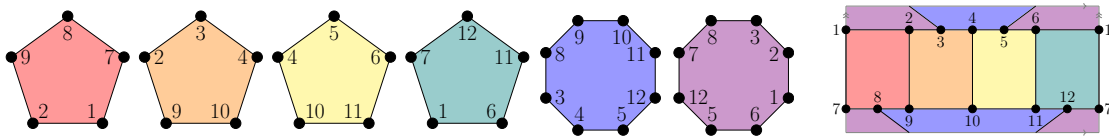
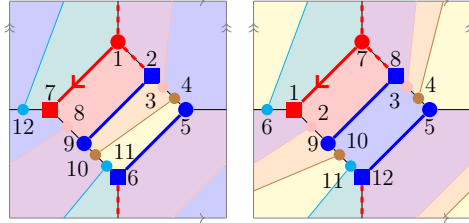


FIGURE 16. Decomposing the 2-embedding of F_{12}

We note that we can decompose the two embeddings of F_{12} resulting from Case 1a into five pentagons, and two octagons. Moreover, we can label the vertices of the two embeddings resulting from Case 1a and decompose the torus as in Figure 16. Hence, the embeddings from this case are equivalent to the known 2-embedding of F_{12} .



Finally, we consider the four pentagons and two octagons below. Identifying vertices with the same label and edges between the same pair of vertices, we obtain the 3-embedding of F_{12} from Figure 11.

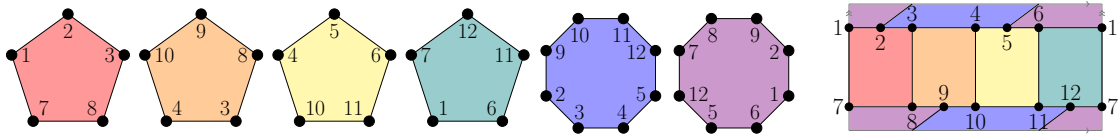
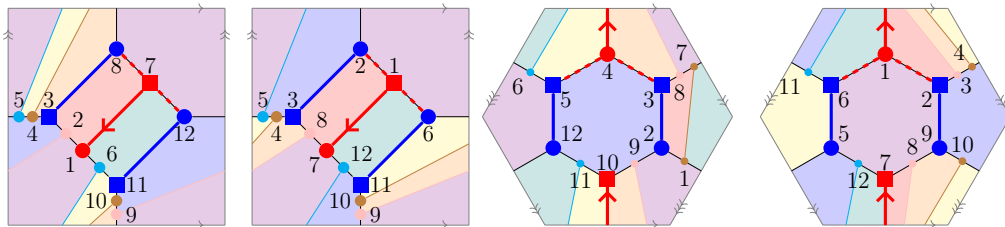


FIGURE 17. Decomposing the 3-embedding of F_{12}

We can decompose the four embeddings of F_{12} resulting from Case 4a and 6a into five pentagons, and two octagons. Moreover, we can label the vertices of these four embeddings and decompose the torus as in Figure 17. Hence, the embeddings from these cases are equivalent to the known 3-embedding of F_{12} .



We can now conclude that there are at most four inequivalent embeddings of F_{12} into the torus, namely the ones depicted in Figure 11. The remarks preceding the proof of Lemma 6 imply that these four embeddings are pairwise inequivalent, finishing the proof.

□

5. TOROIDAL EMBEDDINGS OF F_{13}

Lemma 7. *There are exactly two inequivalent unlabelled embedding of F_{13} into the torus.*

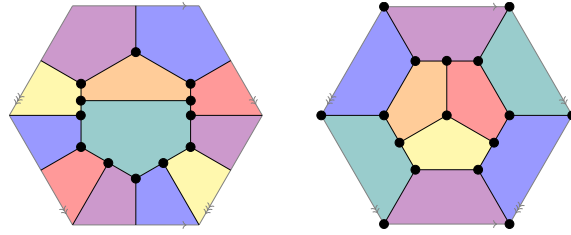
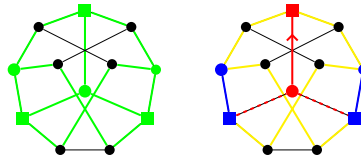


FIGURE 18. The two embeddings of F_{13} into the torus

Remark.

- (1) The embedding on the left has three facial cycles of length five, two facial cycles of length six, and one facial cycles of length nine. In particular, it is the only embedding with a facial 9-cycle and thus cannot be equivalent to the other embedding. We will refer to it as the *9-cycle embedding*.
- (2) The embedding on the right has three facial cycles of length five, and three facial cycles of length seven. In particular, it is the only embedding with a facial 7-cycle. We will refer to it as the *7-cycle embedding*.

Proof. Similar to the other graphs we have analysed in Sections 3 and 4, we fix a subgraph H of F_{13} homeomorphic to $K_{3,3}$ as shown below.



The subdivision of $K_{3,3}$ is shown below, where $K_{3,3}$ is drawn as the Möbius ladder on three rungs. Note that the unlabelled versions of the graphs on the left in Figures 12 and 19 are identical. Once we have the pictured subdivision of $K_{3,3}$, there is a unique way to add the remaining edges to obtain F_{13} by recalling that F_{13} is cubic and has girth five.

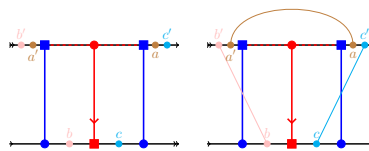
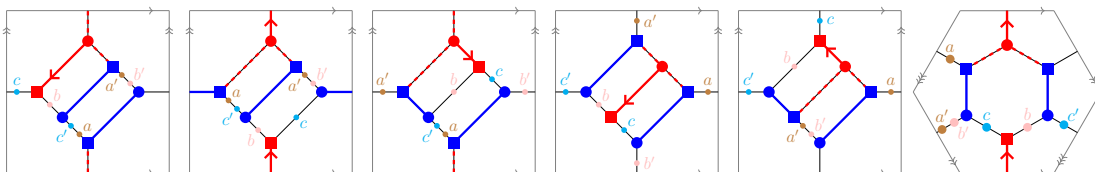


FIGURE 19. Building F_{13} from $K_{3,3}$

In the same way as in the proof of Lemma 6 we get twelve *blue directed edged embeddings* of the subdivision of $K_{3,3}$.



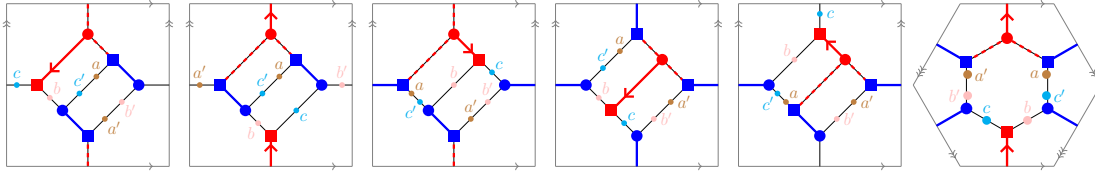


FIGURE 20. Subdivisions of $K_{3,3}$ in F_{13}

The cases are labelled 1a, 2a, etc. across the top row, and 1b, 2b, etc. across the bottom row. We observe that not only are the unlabelled subdivision of $K_{3,3}$ from which we build F_{12} and F_{13} identical, but removing the edge aa' from F_{12} and F_{13} gives homeomorphic graphs. Moreover, the labelled subdivisions from Figures 13 and 20 are closely related. To get from one to the other, one only has to swap vertices a' and b' , and vertices a and c' , respectively. As the case analysis here is similar to the case analysis in the proof of Lemma 6, we omit the details. Cases 1a, 3b, and 4a each result in one embedding of F_{13} , while Cases 5a and 6b each result in two embeddings of F_{13} . See Figures 22 and 24 for pictures of these embeddings. Using the same technique as in the previous sections, we will now show that each of these seven embeddings of F_{13} into the torus is equivalent to one of the two embeddings in Figure 18.

Consider the three pentagons, two hexagons, and one nonagon below. Identifying vertices with the same label and edges between the same pair of vertices, we obtain the 9-cycle embedding of F_{13} from Figure 18.

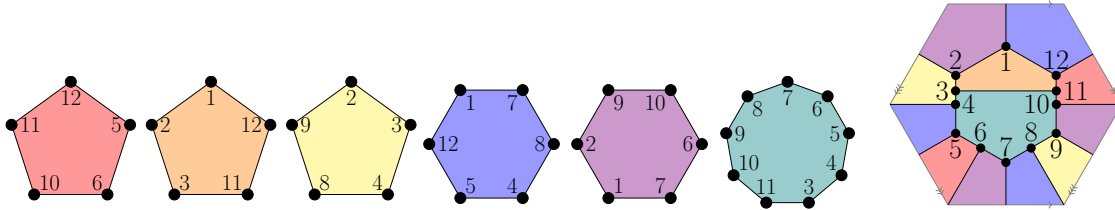


FIGURE 21. Decomposing the 9-cycle embedding of F_{13}

We observe that we can decompose the five embeddings of F_{13} resulting from Cases 1a, 5a and 6b into three pentagons, two hexagons and one nonagon. Moreover, we can label the vertices of these embeddings and decompose the torus as in Figure 21. This implies the existence of a homeomorphism of the torus that realizes an equivalence of the embedding from these cases and the known 6-cycle embedding of F_{12} .

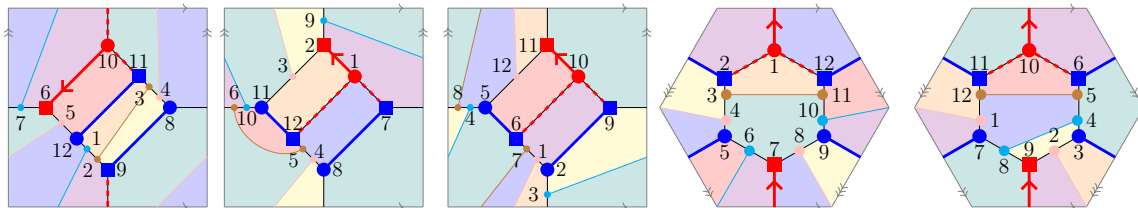


FIGURE 22. Embeddings of F_{13} from Cases 1a, 5a, and 6a

Similarly, consider the three pentagons and three heptagons below. Note that each vertex appears three times, and each edge appears twice. Identifying vertices with the same label and edges between the same pair of vertices, we obtain the 7-cycle embedding of F_{13} from Figure 18.

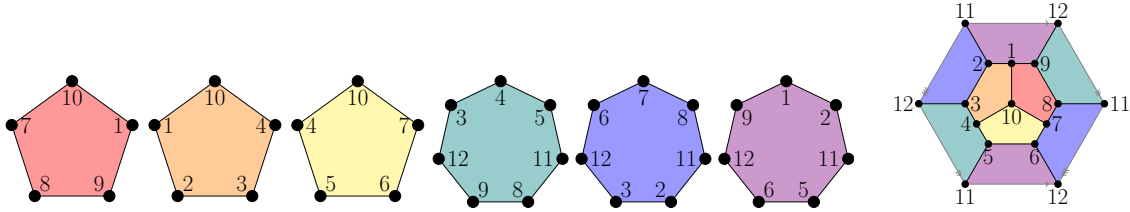


FIGURE 23. Decomposing the 7-cycle embedding of F_{13}

We can decompose the two embeddings of F_{13} resulting from Cases 3b and 4a into three pentagons and four heptagons. Moreover, we can label the vertices of these embeddings and decompose the torus as in Figure 23. Hence, the embeddings from these cases are equivalent to the known 7-cycle embedding of F_{13} .

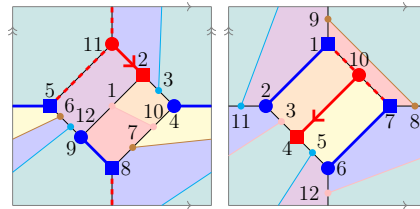


FIGURE 24. Embeddings of F_{13} from Cases 3b and 4a

We can now conclude that there are at most two inequivalent embeddings of F_{13} into the torus, namely the ones depicted in Figure 18. The remarks preceding the proof of Lemma 7 imply that these two embeddings are inequivalent, finishing the proof. □

6. TOROIDAL EMBEDDINGS OF F_{14}

Lemma 8. *There are exactly two inequivalent unlabelled embeddings of F_{14} into the torus.*

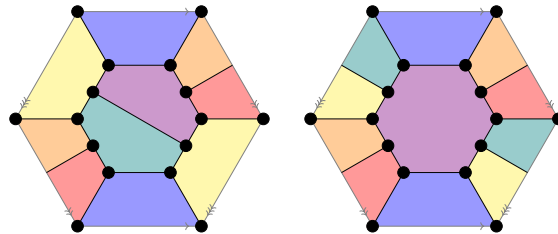
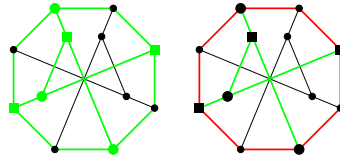


FIGURE 25. The two embeddings of F_{14} into the torus

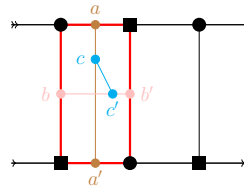
Remark.

- (1) The embedding on the left has two facial cycles of length five, three facial cycles of length six, and one facial cycles of length eight. In particular, it is the only embedding with a facial 8-cycle and thus cannot be equivalent to the other embedding. We will refer to it as the *8-cycle embedding*.
- (2) The embedding on the right has four facial cycles of length five, one facial cycle of length six, and one facial cycle of length ten. In particular, it is the only embedding with a facial 10-cycle. We will refer to it as the *10-cycle embedding*.

Proof. Similar to the previously analysed graphs, we fix a subgraph H of F_{14} homeomorphic to $K_{3,3}$ as shown below.



The subdivision of $K_{3,3}$ is shown below, where $K_{3,3}$ is drawn as the Möbius ladder on three rungs. To build F_{14} , choose one of the facial 4-cycles, subdivide each of its edges once, and connect the new vertices of degree two on disjoint edges. The two new edges then get subdivided once, and the new vertices get connected.



By Lemma 4, there are five inequivalent cycled embeddings $(K_{3,3}, C_4) \hookrightarrow T^2$. As described above, picking a 4-cycle in $K_{3,3}$ completely determines how to build F_{14} . Hence, we analyse the five cases below and check which ones can be extended to an embedding of F_{14} .

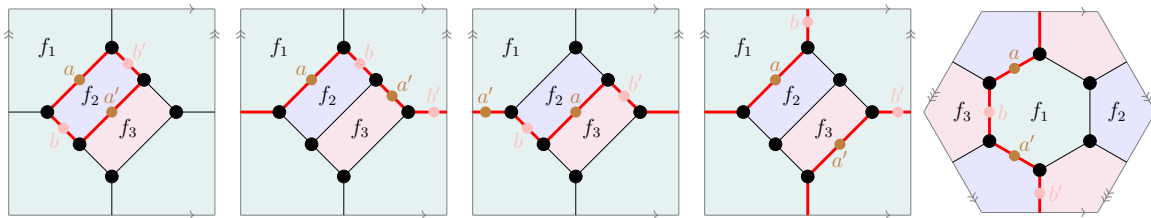
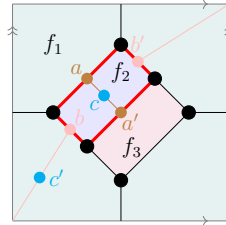


FIGURE 26. Subdivisions of $K_{3,3}$ in F_{14}

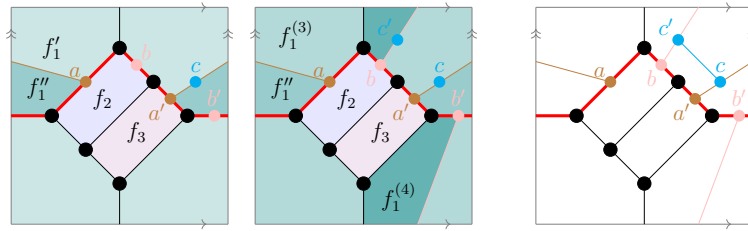
We immediately see that in Case 3 the edge aa' cannot be added. Thus, this embedding does not extend to an embedding of F_{14} .

Note that since all embeddings of $K_{3,3}$ into the torus are cellular, each face is homeomorphic to a disk. Thus, if two vertices are on the boundary of a common face and neither of them appears more than once, there is a unique way to add an edge between the vertices.

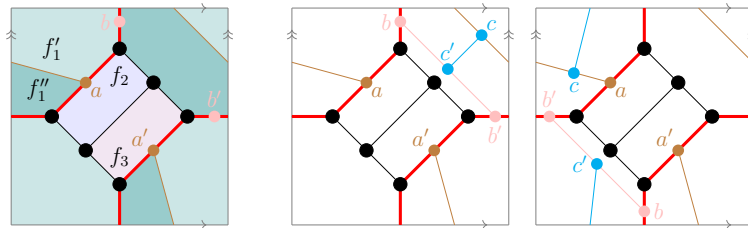
- Case 1: f_2 is the unique face such that the vertices a and a' appear on its boundary, while face f_1 is the unique face such that vertices b and b' appear on its boundary. This leads to vertex c to be in face f_2 , and vertex c' to be in face f_1 . Therefore, we cannot add the edge cc' and the given embedding of a subdivision of $K_{3,3}$ cannot be extended to an embedding of F_{14} .



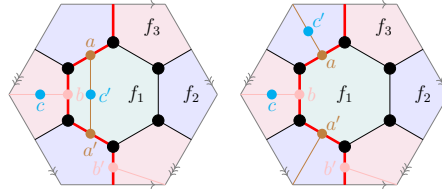
- Case 2: f_1 is the unique face such that the vertices a and a' appear on its boundary, and each vertex appears exactly once. Thus, there exists a unique way to draw the edge aa' . Now, f'_1 is the unique face such that the vertices b and b' appear on its boundary, and each vertex appears exactly once. So, there exists a unique way to draw the edge bb' . Finally, $f_1^{(3)}$ is the unique face such that vertices c, c' appear on its boundary, and they each appear exactly once. Hence, we get the embedding of F_{14} pictured below.



- Case 4: Similar to Case 2, there is a unique way to draw the edges aa' . Now, the vertices b and b' both appear once on the boundary of face f'_1 and once on the boundary of face f''_1 . Hence, there are two ways to draw the edge bb' . For each of the two choices, there is then a unique way to draw the edge cc' , giving the two embeddings of F_{14} pictured below.



- Case 5: f_3 is the unique face such that the vertices b, b' appear on its boundary, and each vertex appears exactly once. So there is a unique way to add the edge bb' . Note that this puts vertex c' into face f_3 . Now, vertices a, a' appear exactly once each on the boundary of f_1 and f_2 . This will lead to vertex c to either be in face f_1 or f_2 . In either case, it is impossible to add the edge cc' , and hence the given embedding of a subdivision of $K_{3,3}$ cannot be extended to an embedding of F_{14} .



Using the same technique as in the previous sections, we will now show that each of these three embeddings of F_{14} into the torus is equivalent to one of the two embeddings in Figure 25.

Consider the two pentagons, three hexagons, and one octagon below. Identifying vertices with the same label and edges between the same pair of vertices, we obtain the 8-cycle embedding of F_{14} from Figure 25.

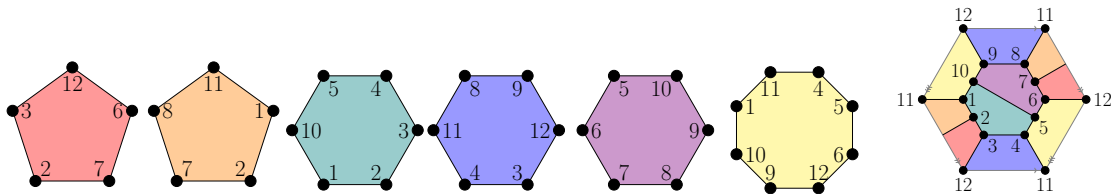
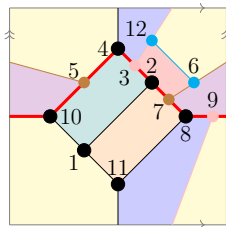


FIGURE 27. Decomposing the 8-cycle embedding of F_{14}

We now observe that we can decompose the embedding of F_{14} resulting from Case 2 into two pentagons, three hexagons, and one octagon. Moreover, we can label the vertices of these embeddings and decompose the torus as in Figure 27. This implies the existence of a homeomorphism of the torus that realizes an equivalence of the embedding from this case and the known 8-cycle embedding of F_{14} .



Similarly, consider the four pentagons, one hexagon and once decagon below. Identifying vertices with the same label and edges between the same pair of vertices, we obtain the 10-cycle embedding of F_{14} from Figure 18.

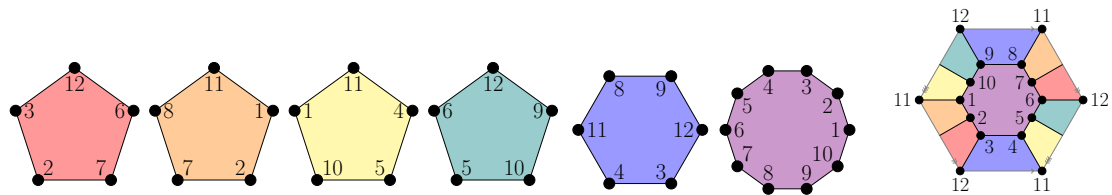
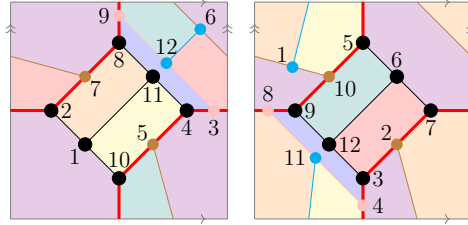


FIGURE 28. Decomposing the 10-cycle embedding of F_{14}

We decompose the two embeddings of F_{14} resulting from Case 4 into four pentagons, one hexagon and once decagon. Moreover, we can label the vertices of these embeddings and decompose the torus as in Figure 23. Hence, the embeddings from this case are equivalent to the known 10-cycle embedding of F_{14} .



We can now conclude that there are at most two inequivalent embeddings of F_{43} into the torus, namely the ones depicted in Figure 25. The remarks preceding the proof of Lemma 8 imply that these two embeddings are inequivalent, finishing the proof. □

7. TOROIDAL EMBEDDINGS OF G_1

Lemma 9. *There are exactly two inequivalent unlabelled embeddings of G_1 into the torus.*

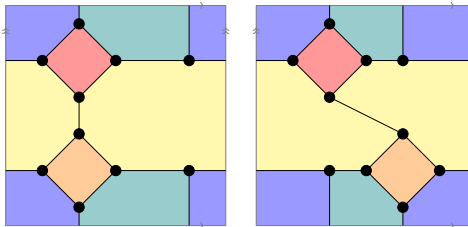
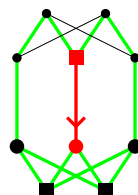


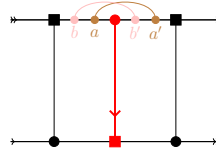
FIGURE 29. Two embeddings of G_1 into the torus

Remark. Both embeddings have two facial cycles of length four, two facial cycles of length six, and one facial cycle of length ten. To distinguish between the two, we consider the facial cycles of length four. Denote these facial cycles in the embedding on the left by C_L and C'_L , and the ones in the embedding on the right by C_R and C'_R . Now we observe that there are two distinct edges connecting a vertex in C_L to a vertex in C'_L , while there is only one edge connecting a vertex in C_R to one in C'_R . As a homeomorphism of the torus would have to map an edge connecting facial 4-cycles to an edge connecting facial 4-cycles, the two embeddings cannot be equivalent. We will refer to the first of these two embeddings as the *2-embedding*, and the other as the *1-embedding*.

Proof. Similar to the other graphs we have analysed in Sections 3 – 6, we fix a subgraph H of G_1 homeomorphic to $K_{3,3}$ as shown below.



The subdivision of $K_{3,3}$ is shown below, where $K_{3,3}$ is drawn as the Möbius ladder on three rungs. Note that the directed edge \vec{e} starts at the unique vertex two of whose incident edges get subdivided twice. Moreover, \vec{e} does not get subdivided. Once we have the pictured subdivision of $K_{3,3}$, there is a unique way to add the remaining edges to obtain G_1 by recalling that G_1 is cubic and has girth four.



By Lemma 2, there are six inequivalent directed edged embeddings $(K_{3,3}, \vec{e}) \hookrightarrow T^2$. As described above, picking one edge in $K_{3,3}$ completely determines how to build G_1 . Hence, we analyse the six cases below and check which can be extended to an embedding of G_1 .

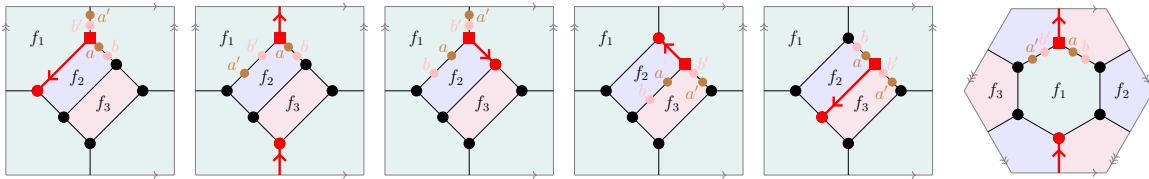
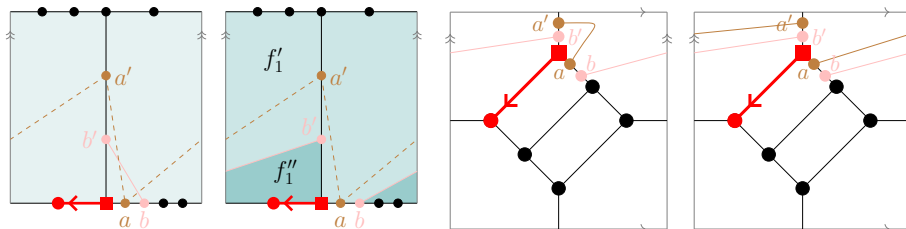


FIGURE 30. Subdivisions of $K_{3,3}$ in G_1

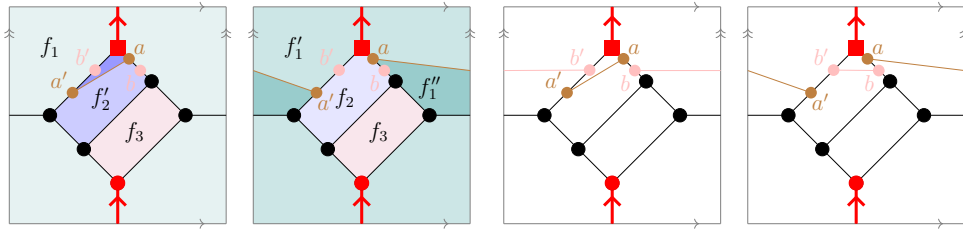
Note that since all embeddings of $K_{3,3}$ into the torus are cellular, each face is homeomorphic to a disk. Thus, if two vertices are on the boundary of a common face and neither of them appears more than once, there is a unique way to add an edge between the vertices.

- Case 1: f_1 is the unique face such that the vertices a and a' appear on its boundary. f_1 is also the unique face with vertices b and b' to appear on its boundary. Moreover, vertices a' and b' appear twice each. Thus, there are two ways to draw the edge bb' , and two ways to draw the edge aa' . It is quick to see that one of the options of adding the edge bb' makes adding the edge aa' impossible (left picture). Thus, we choose the other option. Then there are two ways of drawing the edge aa' as vertex a' appears twice on the boundary of face f'_1 after adding the edge bb' . Hence, we get the two embeddings of G_1 pictured below.

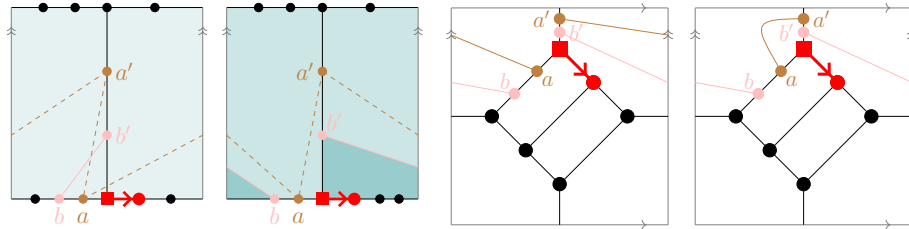


- Case 2: Vertices a and a' are both on the boundary of face f_1 and f_2 . Moreover, they appear exactly once on each boundary. Hence, there is a unique way to connect them through face f_1 , and a unique way to connect them through face f_2 . In both cases, after adding the edge aa' there then is a unique face such that vertices b and

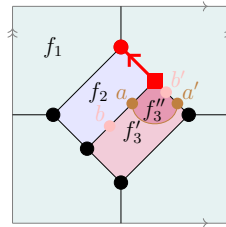
b' appear on its boundary, and moreover each appears exactly once. Hence, we get the two embeddings of G_1 pictured below.



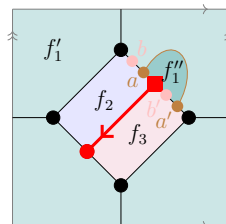
- Case 3: As in Case 1, f_1 is the unique face such that the vertices a and a' appear on its boundary and b and b' appear on its boundary. As a' and b' appear twice, there are two ways to draw the edge bb' , and two ways to draw the edge aa' . Again, one of the options of adding the edge bb' makes adding the edge aa' impossible (left picture). Thus, we choose the other option, and as in Case 1 we see there are two ways of drawing the edge aa' , giving the two embeddings of G_1 pictured below.



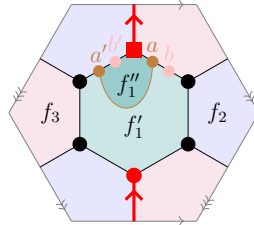
- Case 4: f_3 is the unique face such that the vertices a and a' appear on its boundary, and each appears exactly once. Thus, there is a unique way to draw the edge aa' . However, now there is no face with b and b' on its boundary. Hence, the given embedding of a subdivision of $K_{3,3}$ cannot be extended to an embedding of G_1 .



- Case 5: Similar to Case 4, f_1 is the unique face such that the vertices a and a' appear on its boundary, and each appears exactly once. Thus, there is a unique way to draw the edge aa' . However, now there is no face with b and b' on its boundary. Hence, the given embedding of a subdivision of $K_{3,3}$ cannot be extended to an embedding of G_1 .



- Case 6: f_1 is the unique face such that the vertices a, a' appear on its boundary. f_1 is also the unique face with vertices b, b' to appear on its boundary. Thus, there is a unique way to add each of the edges individually. However, we quickly see that once we have added the edge aa' , it is impossible to add the edge bb' . Hence, the given embedding of a subdivision of $K_{3,3}$ cannot be extended to an embedding of G_1 .



Using the same technique as in the previous sections, we will now show that each of these six embeddings is equivalent to one of the two embeddings in Figure 29.

Consider the two squares, two hexagons, and one decagon below. Identifying vertices with the same label and edges between the same pair of vertices, we obtain the 2-embedding of G_1 from Figure 29.

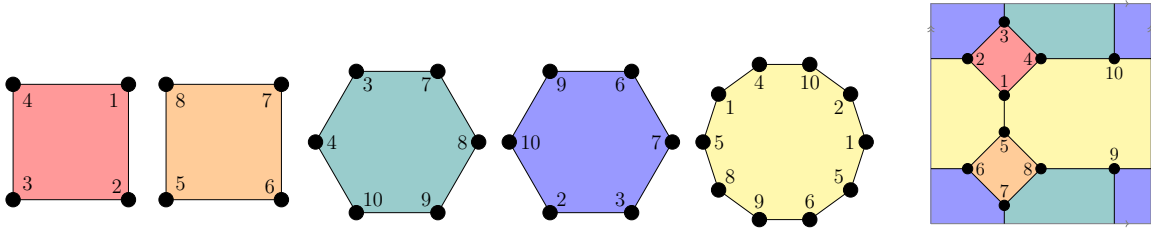
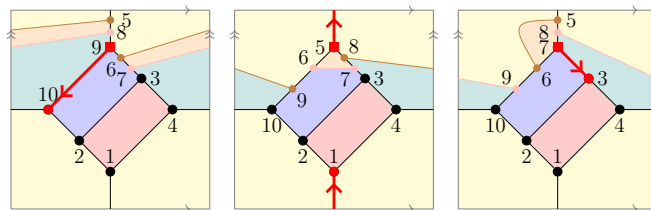


FIGURE 31. Decomposing the 2-embedding of G_1

We now observe that we can decompose each of the embeddings of G_1 resulting from the above cases into two squares, two hexagons and one decagon. Moreover, we can label the vertices of the second embeddings of Cases 1, 2, 3 and decompose the torus as in Figure 32. This implies the existence of a homeomorphism of the torus that realizes an equivalence of the embedding from these cases and the known 1-embedding of G_1 .



Finally, consider the two squares, two hexagons, and one decagon below. Note that each vertex appears three times, and each edge appears twice. Identifying vertices with the same label and edges between the same pair of vertices, we obtain the 1-embedding of G_1 from Figure 29.

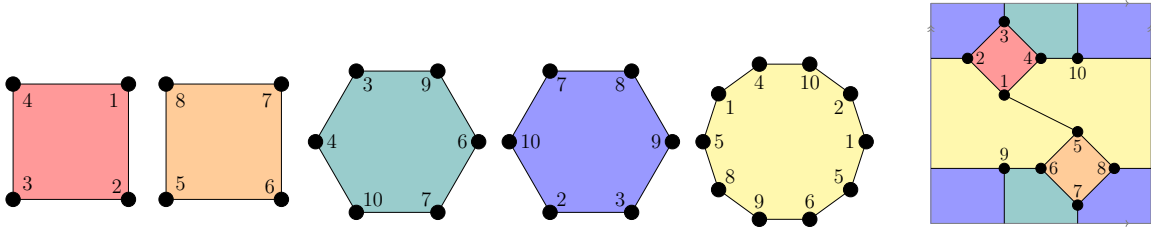
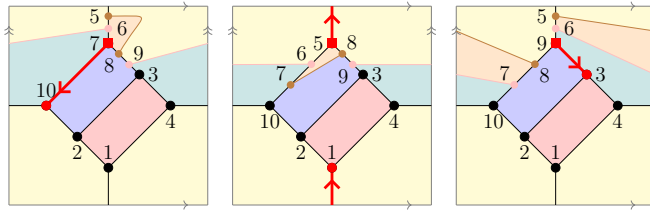


FIGURE 32. Decomposing the 1-embedding of G_1

We can label the vertices of the first embeddings of Cases 1, 2, 3 and decompose the torus as in Figure 31. This implies the existence of a homeomorphism of the torus that realizes an equivalence of the embedding from these cases and the known 2-embedding of G_1 .



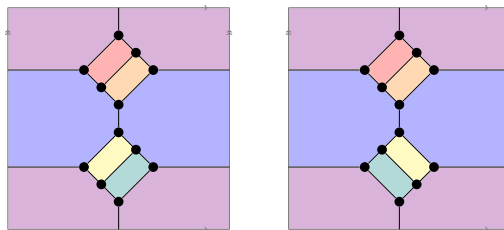
We can now conclude that there are at most two inequivalent embeddings of G_1 into the torus, namely the ones depicted in Figure 29. The remarks preceding the proof of Lemma 9 imply that these two embeddings are inequivalent, finishing the proof.

□

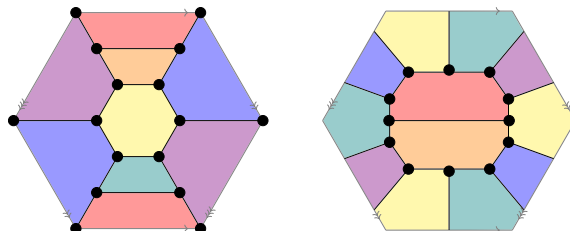
APPENDIX. TABLE OF TOROIDAL EMBEDDINGS OF CUBIC PROJECTIVE PLANE OBSTRUCTIONS

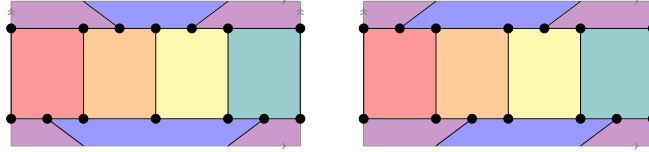
E_{42} has no embeddings into the torus.

F_{11} has the following two inequivalent unlabelled embeddings into the torus.

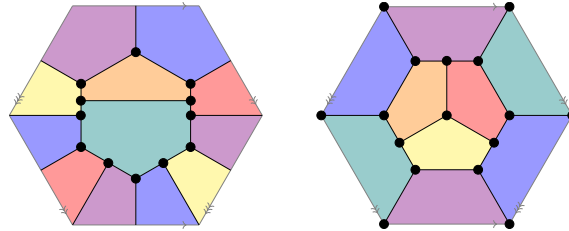


F_{12} has the following four inequivalent unlabelled embeddings into the torus.

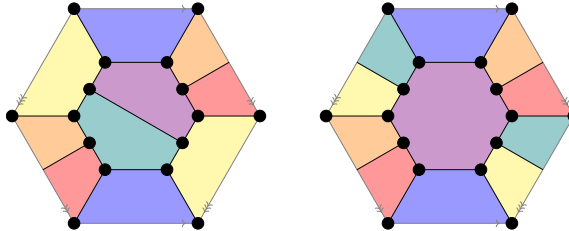




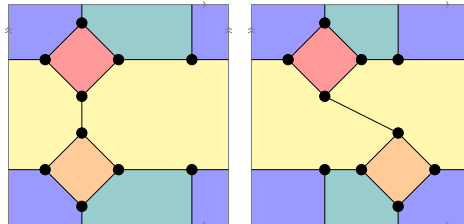
F_{13} has the following two inequivalent unlabelled embeddings into the torus.



F_{14} has the following two inequivalent unlabelled embeddings into the torus.



G_1 has the following two inequivalent unlabelled embeddings into the torus.



REFERENCES

[Arc81] Dan Archdeacon. A Kuratowski theorem for the projective plane. *Journal of Graph Theory*, 5(3):243–246, 1981.

[BHK62] Joseph Battle, Frank Harary, and Yukihiro Kodama. Additivity of the genus of a graph. *Bulletins of the American Mathematical Society*, 68:565–568, 1962.

[Cha02] John Chambers. Hunting for torus obstructions. Master’s thesis, University of Victoria, 2002.

[FHRR95] J.R. Fiedler, J.P. Huneke, R.B. Richter, and N. Robertson. Computing the orientable genus of projective graphs. *Journal of Graph Theory*, 20(3):297–308, 1995.

[GH75] Henry H. Glover and John P. Huneke. Cubic irreducible graphs for the projective plane. *Discrete Mathematics*, 13(4):341–355, 1975.

[GHW79] Henry H. Glover, John P. Huneke, and Chin San Wang. 103 graphs that are irreducible for the projective plane. *Journal of Combinatorial Theory, Series B*, 27(3):332–370, 1979.

[GKN03] Andrei Gagarin, William Kocay, and Daniel Neilson. Embeddings of small graphs on the torus. *Cubo, A Mathematical Journal*, 5(2):351–371, 2003.

[KK17] William L. Kocay and Donald L. Kreher. *Graphs, Algorithms, and Optimization*. CRC Press, Second edition, 2017.

[Kur30] Kazimierz Kuratowski. Sur le problème des courbes gauches en Topologie. *Fundamenta Mathematicae*, 15(1):271–283, 1930.

[KWW] Lee Kennard, Michael Wiemeler, and Burkhard Wilking. Positive curvature, torus symmetry, and matroids. arXiv:2212.08152.

- [Moh93] Bojan Mohar. Projective planarity in linear time. *Journal of Algorithms*, 15(3):482–502, 1993.
- [MT01] Bojan Mohar and Carsten Thomassen. *Graphs on Surfaces*. The Johns Hopkins University Press, 2001.
- [MW18] Wendy Myrvold and Jennifer Woodcock. A large set of torus obstructions and how they were discovered. *The Electronic Journal of Combinatorics*, 25(1), 2018.

DEPARTMENT OF MATHEMATICS, SYRACUSE UNIVERSITY, SYRACUSE, NY USA

Email address: `mkrame04@syr.edu`